The Rheology of Colloidal and Noncolloidal Food Dispersions

D. B. GENOVESE, J. E. LOZANO, AND M. A. RAO

ABSTRACT: Rheological data on a food together with data on its composition and structure or microstructure should lead to understanding the interrelationships between them. A number of foods are dispersions of solids in liquids, liquids in liquids, or gas in liquids. The dispersed particles may be colloidal in nature with dimensions < 10 μm, or larger noncolloidal particles (> 10 μm). For both colloidal and noncolloidal dispersions (either in dilute or concentrated regimes), several theoretical equations exist that provide insights into the role of key rheological parameters, such as particle volume fraction and size, interparticle forces, and fractal dimension on their viscosity, yield stress, and modulus. When theoretical models cannot be easily applied to foods with complex structures, structural analysis and structure-based models provide insight into the role of solids loading and interparticle bonding on rheological behavior. In this review, recent studies on colloidal and noncolloidal food dispersions in which theoretical models as well as structural analysis were employed are discussed.

Keywords: colloidal, dispersions, food, noncolloidal, rheology

Introduction

Processed foods are edible structures that are created as a result of the responses of proteins, mono and polysaccharides, and lipids in aqueous media to different processing methods such as thermal processing, homogenization, and other physical treatments. Most, if not all, of those responses are physical in nature. The measured rheological responses occur at the macroscopic level. However, they are affected by the changes and properties at the molecular and microscopic level. A major challenge is to establish links between the macroscopic rheological properties with changes at the molecular and microscopic level (Rao 2006). Rheological data on a food together with data on its composition and structure or microstructure should lead to understanding the interrelationships between them. In turn, such knowledge should lead to the improvement in food quality through creation of foods with desirable structures and rheological behavior.

Many foods are dispersions of either solids in a liquid medium, usually an aqueous solution, or of liquid droplets in another liquid, named emulsions.

Three kinds of forces coexist to various degrees in flowing dispersions: hydrodynamic, Brownian, and colloidal forces. Hydrodynamic forces arise from the relative motion of particles to the surrounding fluid. The Brownian force is the ever-present thermal randomizing force. Colloidal forces are potential forces and are elastic in nature (Zhou and others 2001; Qin and Zaman 2003). The relative magnitude of these forces and, therefore, the bulk rheology depend on the particle size. Brownian motion and interparticle forces quickly equilibrate for sub-nanometer-size dispersions, while hydrodynamic forces dominate for particles larger than approximately 10 μm. For particles in the intermediate range the flow behavior is determined by a combination of hydrodynamic forces, Brownian motion, and interparticle forces (Russel 1980; Qin and Zaman 2003). Consequently, dispersions may be classified according to the size and nature of the particles in them (Table 1).

Colloidal dispersions may be defined as polyphasic or heterogeneous systems where the dispersed phase is subdivided into discrete units (particles/droplets) that are large compared to simple molecules, but small enough so that interfacial and inertial forces are significant in governing system properties (Sennet and Olivier 1965). The size range of colloidal (or Brownian) particles is not defined rigidly, but typically considered to be 1 nm to 10 μm (Russel and others 1989; McClements 1999; Qin and Zaman 2003), as for example cloudy fruit juices, milk, soy protein suspensions, and mayonnaise (a colloidal emulsion). Brownian motion promotes collisions between pairs of colloidal particles, while interparticle forces determine if 2 colliding particles aggregate or not.

The particle arrangements in colloidal systems depend on the volume occupied by the particles in relation to the total volume, that is, the particle volume fraction, ϕ. At low ϕ, the mean distance between particles is large compared to particle radius. Thus, particles are able to move freely throughout the medium driven by Brownian forces. This regime ($\phi \to 0$) is considered as the dilute limit. As ϕ increases, hydrodynamic interactions and the probability of collision between particles become important. As a consequence, the Brownian motion of each particle is hindered by the presence of the other ones. In this region, the suspension is considered to be concentrated (Quemada and Berli 2002).

Colloidal suspensions can be either dispersed or flocculated, depending on the magnitude of particle–particle interaction energy and particle concentration. Two limit cases are usually considered for the mechanism of aggregation: perikinetic aggregation, where the particle encounters are due to Brownian motion, and orthokinetic aggregation, where the collisions are caused by the gradient velocity field. This last mechanism dominates for particles of micrometer size and larger (Berli and others 1999b).

In weakly flocculated dispersions, particles form a volume-spanning network. For aggregation resulting from long-range attractions, deformation of the network changes the relative positions of the particles, thereby increasing the total potential energy of the system and producing an interparticle force tending to restore the

MS 20060509 Submitted 9/13/2006, Accepted 11/14/2006. *Authors Genovese and Lozano are with PLAPIQUI (UNS-CONICET), Camino La Carrindanga Km 7, 8000 Bahía Blanca, Argentina. Author Rao is with Dept. of Food Science and Technology, Cornell Univ., Geneva, NY 14456-0462, Direct inquiries to author Genovese (E-mail: dgenovese@plapiqui.edu.ar).*

doi: 10.1111/j.1750-3841.2006.00253.x

Table 1—Classification of dispersions

Particle size/nature		Forces governing viscosity
Polymers approximately 1 nm	Molecular/colloidal	Dilute: intermolecular-Brownian Concentrated: Entanglements and Reptation
1 nm-10 μm[a]	Microscopic/colloidal	Low $\dot{\gamma}$: Hydrodynamic-interparticle-Brownian High $\dot{\gamma}$: Hydrodynamic
10 μm-100 μm[a]	Microscopic/noncolloidal	Hydrodynamic
$>$ 100 μm	Macroscopic/noncolloidal	Hydrodynamic

[a]Food dispersions covered in this review.

equilibrium structure. The nonequilibrium nature of the structure gives a complex, history-dependent rheological behavior (Russel and others 1989). A colloidal gel is a special state of strongly flocculated systems where a continuous network of particles (often < 0.1 μm) is formed by aggregation, with the resulting suspension having a very high viscosity and a finite shear modulus.

Several foods contain microscopic particles that are >10 μm and up to approximately 100 μm (for example, chocolate, fruit purees and sauces, starch and vegetable pastes); some of them may be flocs or aggregates of colloidal particles. For such large particles, Brownian motion and interparticle forces are negligible compared to hydrodynamic forces. However, nonhydrodynamic parameters such as particle shape, particle size and size distribution, particle deformability, and liquid polarity could affect the structure and the resulting flow behavior (Tsai and Zammouri 1988). Such dispersions have been called simply "noncolloidal" or non-Brownian.

Other foods contain macroscopic particles (>100 μm), for example, vegetable or cream soups, fruits in syrups or yogurts, dressings or sauces with seeds, and pasta or meat in sauces. Gondret and Petit (1997) referred to dispersions of glass spheres of diameter 45 to 450 μm as macroscopic. Those food dispersions are usually considered to be liquid/particle mixtures, and sometimes the liquid itself is a colloidal dispersion (Martínez-Padilla 2005). In this case, when the particle size has atomic dimensions, the system consists of a molecular or ionic dispersion, although strictly speaking it is a 1-phase system (Sennet and Olivier 1965).

It should be emphasized that most foods are complex polydisperse systems that may contain particles from a broad size range (that is, both microscopic and macroscopic particles) immersed (or even imbibed) in an aqueous (or lipid) medium, which in turn may be a molecular dispersion itself. The rheological behavior of such systems has been covered by several groups, including Rao and coworkers (Vitali and Rao 1984; Tanglertpaibul and Rao 1987; Yoo and Rao 1996).

In addition to solid–liquid and liquid–liquid systems, liquid food foams are biphasic systems where a gas bubble phase is dispersed in a continuous liquid phase, with the gas–liquid interface being under tension. Their complex rheological behavior is influenced by many factors, such as air phase volume, liquid phase viscosity, interfacial tension and viscosity, bubble size, size distribution, and shape (Herzhaft 1999; Vernon-Carter and others 2001; Thakur and others 2003). There are also solid food foams (typically cooked products such as breads or cakes), which consist of a discontinuous air phase dispersed in a continuous solid phase. Solid foams are elastic or plastic materials. Their mechanical (rheological) behavior is beyond the scope of this work, but we may mention that it is primarily dependent on the physical properties of the solid phase and the bulk density of the material (Pernell and others 2002).

The present review is focused on microscopic colloidal and noncolloidal food dispersions. The objective is to discuss the role of structure on their rheological properties in terms of theoretical models and structural analysis. Measurement of rheological properties has been well covered in texts such as those of Steffe (1996) and Rao (1999); therefore, they are not covered here.

Theoretical Rheological Models and Their Application

Theoretical models are derived from fundamental concepts, and they provide valuable guidelines on understanding the role of structure. They indicate the factors that influence a rheological parameter. As mentioned, the viscosity of colloidal dispersions is affected by interparticle forces and Brownian motion at low shear rates, while hydrodynamic forces dominate at high shear rates (Berli and others 1999a). On the other hand, the viscosity of noncolloidal dispersions is governed by hydrodynamic forces within all the range of shear rates.

Viscosity models for noncolloidal dispersions

The hydrodynamic disturbance of the flow field induced by solid particles in liquid media leads to an increase in the energy dissipation and an increase in viscosity (Zhou and others 2001). The relative viscosity of dispersions of solid particles in a liquid medium is defined as

$$\eta_r = \left(\eta / \eta_s\right) \tag{1}$$

where η is the viscosity of the dispersion, and η_s is the viscosity of the continuous phase. In general, η_r of dispersions of rigid, noninteracting spherical particles (hard-sphere systems) depends on the volume fraction, ϕ, and the intrinsic viscosity, $[\eta]$, of the dispersed solids (Eq. 2 and 3). At low particle concentrations (in the dilute regime), it is described by the well-known Einstein's equation

$$\eta_r = 1 + [\eta]\,\phi \tag{2}$$

Theoretically, $[\eta]$ depends on particle shape, being 2.5 for rigid spheres (Barnes 2000).

One relationship derived for concentrated dispersions is the widely used Krieger–Dougherty equation (Krieger and Dougherty 1959)

$$\eta_r = \left(1 - \frac{\phi}{\phi_m}\right)^{-[\eta]\phi_m} \tag{3}$$

where ϕ_m is the maximum packing fraction of solids. Although the theoretical ϕ_m value of monodisperse spheres is 0.74 (in a face-centered cubic array), experimental observations have shown that loose random packing is close to 0.60, and that dense random packing is close to 0.64 (Quemada and Berli 2002; Servais and others 2002; Qin and Zaman 2003).

Effect of particle shape and particle size distribution. When the particles are nonspherical there is an extra energy dissipation and consequently an increase in the viscosity. In dilute dispersions

this increase is reflected by the intrinsic viscosity in Einstein equation (Eq. 2). Simple formulas has been derived by Barnes (2000) as $[\eta] = 0.07q^{5/3}$ for rod-like (prolate) particles, and $[\eta] = 0.3q$ for disk-like (oblate) particles, where q is the axial ratio. The effect of particle shape on concentrated suspensions was studied by Kitano and others (1981), who proposed a modification of the Krieger–Dougherty relationship (Eq. 3) for suspensions of nonspherical particles

$$\eta_r = \left(1 - \frac{\phi}{\beta}\right)^{-2} \tag{4}$$

where β is an adjustable parameter whose value decreases as the aspect ratio (L/D) of the suspended particles increases; for example, when L/D = 1 (smooth spheres) $\beta = \phi_m$, and when $6 < L/D < 8$ (rough crystals) $\beta = 0.44$ (Metzner 1985; Rao 1999).

Equation 3 is valid for monomodal spherical particles. For suspensions of polydispersed spherical particles in Newtonian fluids, ϕ_m is higher since small particles may occupy the space between the larger particles. Under flow conditions, the small particles act as a lubricant for the flow of the larger particles, thereby reducing the overall viscosity (Servais and others 2002; Martínez-Padilla 2005). In other words, for a given particle concentration (ϕ), the viscosity decreases at increasing polydispersity (particle size distribution width). Farris (1968) assembled many monomodal distributions and showed that the overall resulting viscosity was the product of the relative viscosity associated with each discrete unimodal size distribution, $\eta_{ri}(\phi_i)$, assuming no interactions between the particles of different class sizes

$$\eta_r = \prod_{i=1}^{n} \eta_{r_i}(\phi_i) \tag{5}$$

Effect of particle deformability. At high concentrations, deformable particles can accommodate each other at rest and squeeze past each other during flow, increasing ϕ_m and reducing $[\eta]$ in Eq. 3, resulting in a lower viscosity (Barnes 2000). Often, the data necessary to apply a theoretical model are not easy to obtain. For example, in a starch dispersion of a specific concentration, c, ϕ changes during heating of the dispersion; it has a low value in the ungelatinized state and it increases continuously to a maximum value. After the maximum value has been attained, on further heating, the volume fraction of a native starch often decreases substantially while that of a cross-linked starch remains nearly the same (Yang and Rao 1998; Rao 1999; Tattiyakul and Rao 2000). Because of their deformable nature, it is difficult to determine volume fraction of starch dispersions accurately and it is preferable to work with starch granule mass fraction, (cQ), where c is dry starch concentration, w/w, and Q is the mass of hydrated starch granules per unit weight of dry starch.

Yang and Rao (1998) and Liao and others (1999) obtained complex viscosity, η^*, versus temperature data of a starch dispersion at several oscillatory frequencies (not shown here). Because the profiles were similar in shape, by choosing an arbitrary reference frequency (ω_r), all the η^*-temperature curves at the different frequencies were reduced to a single master curve of reduced complex viscosity η^*_R as in Figure 1.

The shape of the curve in Figure 1 reflects the aforementioned changes in the volume fraction of starch granules. Initially at low temperatures, the granules are in the raw state and the volume fraction is low. As the granules are heated they swell due to water absorption (segment A-B-C), the volume fraction increases and reaches a maximum value (C). With further heating, the granules rupture and disintegrate, resulting in a gradual decrease in the volume fraction of the granules in the dispersion (segment C-D). The rupture of granules also results in the release of amylose that contributes to the viscosity of the continuous phase of the starch dispersion. Thus, in Figure 1, the segment C-D is not a mirror image of the segment ABC. The leached amylose and the granule remnants contribute to a viscosity at point D that is higher than that at point A.

Viscosity models for colloidal dispersions

In stable colloidal dispersions, repulsive forces keep neighboring particles away from each other. Therefore, for flow to occur particles must be forced to move against the force fields of the other particles, demanding an extra energy (Berli and others 1999a). The predictive models for the viscosity of colloidal dispersions are divided into 2 categories based on their scaling technique. One is the separation of contributions method, in which the contributions from individual factors are separated from each other. The other is the effective volume fraction method, in which all the contributions from different factors are lumped into 1 factor, the effective maximum packing fraction (Qin and Zaman 2003).

In the separation of contributions method, the relative viscosity of a colloidal dispersion has been modeled (Ogawa and others 1997; Quemada and Berli 2002) as the sum of a "hard-sphere" contribution (η_r^{hs}) and a "colloidal forces" contribution (η_r^{cf})

$$\eta_r = \eta_r^{hs} + \eta_r^{cf} \tag{6}$$

The term η_r^{hs} is considered to be the relative viscosity of an ideal dispersion of hard spheres or, more generally, the relative viscosity of a noncolloidal dispersion of rigid particles. Thus, it can be calculated by selecting the appropriate expression from Eq. 2 to 5.

The term η_r^{cf} involves the increase in viscosity due to interparticle colloidal forces. They can be classified as attractive (including van der Waals, electrostatic attractive, hydrophobic, bridging, and depletion) and repulsive (including electrostatic repulsive, steric, hydration, and structural) forces (McClements 1999; Zhou and others 2001). The total or net interaction potential (U) between pairs of particles as a function of the interparticle distance (r) may be predicted by the extended DLVO theory.

Charged particles in an electrolyte present an arrangement of charges in the interface called the electrical double layer (EDL). The distortion of the EDL by the shear field leads to an increase in the

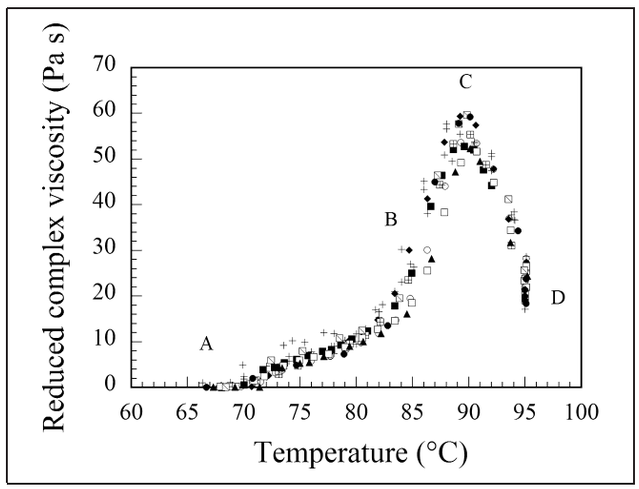

Figure 1 — Change of reduced complex viscosity of a cornstarch dispersion during heating, due to granule swelling and rupture. Master curve of experimental data at different oscillatory frequencies and heating rates. Reprinted from Yang and Rao (1998), with permission from Blackwell Publishing.

viscosity due to increased energy dissipation. This effect was first considered by Smoluchowski and is called the primary electroviscous effect (Hidalgo-Álvarez and others 1996; Rubio-Hernández and others 2004). For dilute dispersions of spherical particles, it appears as a correction p, the primary electroviscous coefficient, to the Einstein equation (Eq. 2), such that combined with Eq. 6 gives

$$\eta_r^{cf} = 2.5\,p\,\phi \tag{7}$$

The coefficient p is a function of the potential in the slipping plane or ζ–potential (a measure of the particle surface potential), and the relative size of the particle radius (a) with respect to the thickness of the EDL, calculated as the Debye length (κ^{-1}). Several theoretical expressions have been derived for p (see, for example, Hidalgo-Álvarez and others 1996; Rubio-Hernández and others 2004).

However, Eq. 7 only considers the contribution of electrostatic repulsive forces to the viscosity. Genovese and Lozano (2006) proposed a more general, semiempirical expression for η_r^{cf} in terms of the maximum net repulsive potential between pairs of particles (U_{Max}), also known as the energy barrier or activation energy

$$\eta_r^{cf} = \alpha\left(\frac{U_{Max}}{k_B T}\right)\phi \tag{8}$$

where α is a dimensionless proportionality constant, k_B is Boltzmann's constant, and T is the absolute temperature. The value of U_{Max} predicts the stability of colloidal dispersions, and is obtained at the maximum of the $U(r)$ curve.

Figure 2 shows the 3 components of Eq. 6 as a function of ϕ for cloudy apple juice from 10 to 50° Brix (Genovese and Lozano 2006). Values of η_r^{cf} were obtained by difference between empirical η_r values and theoretical η_r^{hs} values from Eq. 2. Values of U_{Max} were obtained from the balance between van der Waals, electrostatic, and hydration interparticle forces. By applying Eq. 8, the value $\alpha = 0.483$ was obtained.

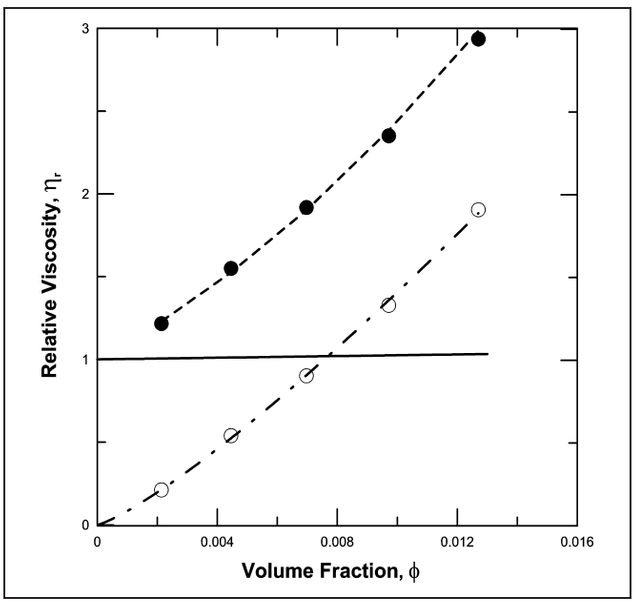

Figure 2—Cloudy apple juice relative viscosity compared with particle volume fraction: experimental (●), and predicted with Eq. 6 (dashed line); theoretical hard-sphere contribution, Eq. 2 (full line); colloidal-forces contribution: semi-empirical values (○), and fitted with Eq. 8 (dashed-dotted line). Reprinted from Genovese and Lozano (2006), with permission from Elsevier.

Figure 3 shows $\eta_r^{cf}(\phi)$ of cloudy apple juice at different pHs and ionic strengths (Benítez and others 2007). Values of U_{Max} were obtained combining the extended DLVO theory and turbidity experimental data. A unique value of $\alpha = 0.267$ was obtained from Eq. 8 for all samples.For concentrated colloidal suspensions, Ogawa and others (1997) derived the following expression based on the theory of activation processes:

$$\eta_r^{cf} = c_1\phi\exp\left(\frac{U_{Max}}{k_B T} - \frac{c_2 d^3 \sigma_p}{\phi \cdot k_B T}\right) \tag{9}$$

where c_1 and c_2 (theoretically $\pi/6$) are numerical constants, d is the particle diameter, and σ_p (approximately 0 for low shears) is the particle stress (as in Eq. 32 also).

In the effective volume fraction method, it is considered that repulsive forces keep particles apart from one another, thus increasing their effective radius from a to a_{eff}. Consequently, the effective volume fraction is given as

$$\phi_{eff} = \phi\left(\frac{a_{eff}}{a}\right)^3 \tag{10}$$

In this context, the viscosity of a colloidal dispersion can be simply obtained by replacing ϕ by ϕ_{eff} in a hard-sphere viscosity equation, like Eq. 3 (Quemada and Berli 2002)

$$\eta_r = \left(1 - \frac{\phi_{eff}}{\phi_m}\right)^{-[\eta]\phi_m} \tag{11}$$

By allowing a_{eff} to be shear-dependent, Buscall (1991, 1994) found an approximate theoretical expression

$$\frac{U(2a_{eff})}{k_B T} = k\left(\frac{\sigma \cdot a_{eff}^3}{k_B T \cdot K(\phi_{eff})} + 1\right) \tag{12}$$

where k approximately $\frac{1}{2}$ and $K(\phi_{eff}) = 0.016 + 0.52\phi_{eff}$ are phenomenological factors.

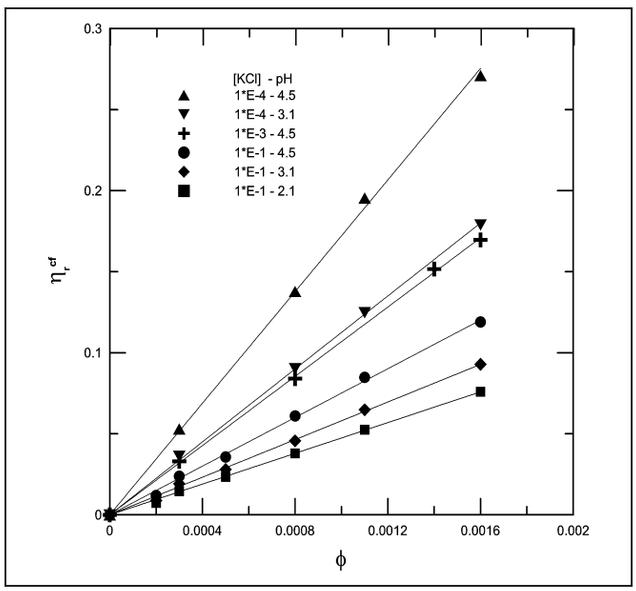

Figure 3—Effect of particle volume fraction on the colloidal forces contribution to relative viscosity, for different liquid medium conditions. Experimental data (symbols) fitted with Eq. 8 (full lines). Reprinted from Benítez and others (2007), with permission from Elsevier.

Aggregating colloidal dispersions and microgel suspensions. The aggregation of colloidal particles leads to the formation of fractal structures, that is, highly branched aggregates. A fractal dimension indicates the degree to which an image or object outline deviates from smoothness and regularity. The term fractal was coined by Mandelbrot (1982), who introduced dimensions "between" the conventional Euclidean dimensions of 1, 2, and 3 in order to describe structures that are not Euclidean lines, surfaces, or solids.

Berli and others (1999) proposed a viscosity equation for an aggregating soy suspension by using the modified Krieger–Dougherty equation (Eq. 3)

$$\frac{\eta}{\eta_m} = \left[1 - \frac{\phi}{\phi_m} N^{(3-D_f)/D_f}\right]^{-2} \tag{13}$$

where η_m is the viscosity of the medium filling the space between the aggregates (instead of η_s), D_f is the fractal dimension of the aggregates, and N is the averaged number of particles in a cluster given by the expression

$$N = 1 + \bar{k}_a (t - t_0) \tag{14}$$

where t_0 is the initial time at which $N \approx 1$, and $\bar{k}_a$ the aggregation rate constant. Combining Eq. 13 and 14 it is possible to measure the degree of aggregation of a suspension (and to estimate the value of D_f) from viscosity-time data.

Microgel suspensions are particles composed of a central zone of cross-linked polymer and an external layer of polymer chains. Berli and Quemada (2000) proposed the following model for these systems

$$\eta(\sigma) = \eta_\infty \left(\frac{\sigma/\sigma_c + 1}{\sigma/\sigma_c - \chi}\right)^2 \tag{15}$$

$$\sigma_c = \frac{k_B T}{a_{hs}^3}\left(1 + \frac{U(2a_{hs})}{k_B T}\right) \tag{16}$$

$$\chi = (\phi/\phi_0 - 1)/(1 - \phi/\phi_\infty) \tag{17}$$

where σ_c is the critical shear stress, χ is a rheological index, a_{hs} is the equivalent hard-sphere radius, which involves the core radius plus the hydrodynamic thickness of the polymer layer, and ϕ_0 and ϕ_∞ are the maximum packing fractions for $\sigma \to 0$ and $\sigma \to \infty$, respectively.

Modulus of colloidal gels of fractal flocs

Shih and others (1990) developed a scaling relationship to explain the elastic properties of colloidal gels by considering the structure of the gel network to be a collection of close packed fractal flocs of colloidal particles. At high particle concentrations, the links between flocs have lower elastic constant than the flocs themselves. This regime should be applicable to gels that are well above the gelation threshold (Shih and others 1990), where the elastic modulus, G', is related to the particle volume fraction (ϕ) by the following relationship:

$$G' \propto \phi^{(D-2)/(D-D_f)} \tag{18}$$

where D is the Euclidean dimension of the network—usually 3.

Russel and others (1989) pointed out that the fractal dimension reflects the internal structure of the flocs and depends on the mode of aggregation. In rapid flocculation, $D_f = 1.75$ for cluster–cluster aggregation, and $D_f = 2.5$ for particle–particle aggregation. On the other hand, slow flocculation allows particles to penetrate further into the floc and rearrange its configuration before sticking, thus increasing D_f to approximately 2.0 and 3.0, respectively.

Fractal dimension of food dispersions. Genovese and Rao (2003a) studied dispersions of 2 starches that were substantially different from each other: a cross-linked waxy maize (CLWM) and tapioca, a tuber starch, with 19.3% amylose. The volume fraction occupied by the starch granules was calculated as the granule mass fraction, that is, $\phi = cQ$. From plots (not shown here) of elastic modulus (G') compared with oscillatory frequency (ω) of the starch dispersions the plateau equilibrium values, G'_0, were determined (Shih and others 1990). The equilibrium G'_0 values obtained for CLWM and tapioca starch dispersions were plotted against ϕ (Figure 4). The double logarithmic plot resulted in reasonable straight lines ($R^2 \geq 0.95$) for both starches, fulfilling the power law relationship inferred by Eq. 18. From the slope of the lines, the fractal dimensions of the 2 types of starch granules were calculated to be $D_f = 2.81$ for CLWM and $D_f = 2.79$ for tapioca, respectively. This was interpreted as both starches having granules with highly convoluted surfaces. The higher G'_0 values of CLWM starch dispersions were attributed to the higher rigidity of their granules (Genovese and Rao 2003a). Studies on fractal dimension of a number of foods, some of them based on rheological data, have been reported and the values obtained, listed in Table 2, illustrate typical magnitudes.

Yield stress models

In general, the magnitude of the yield stress increases with increasing particle volume fraction, decreasing particle size, and increasing magnitude of interparticle forces (Poslinski and others 1988). It has been claimed that yield stress will not occur in a hard-sphere system until the maximum packing fraction is reached (Zhou and others 2001). Most investigations have established and/or quantified yield stresses in suspensions of interacting (colloidal or surface active) particles. Just a few works (Husband and others 1993; Marquez and others 2006) were found on yield stress determination of highly concentrated noncolloidal suspensions. In calcium carbonate filled polyisobutylene suspensions (27 μm in diameter, 0%-57% volume fractions), Husband and others (1993) found a proportional dependence of the yield stress with particle volume fraction.

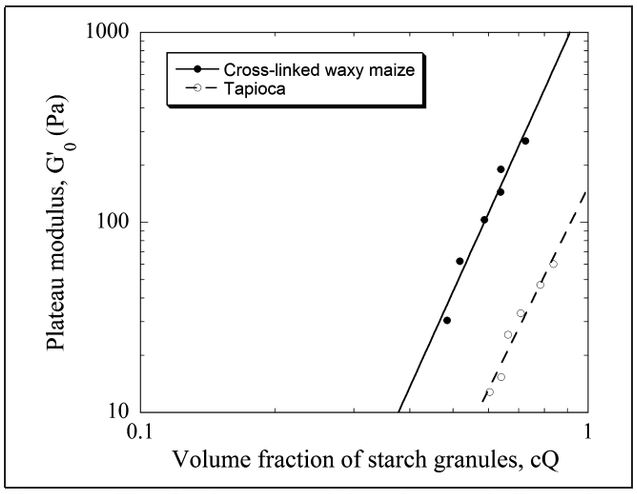

Figure 4 — Elastic plateau modulus of 2 starch dispersions as a function of their granules volume fraction. Experimental data (symbols) fitted with Eq. 17. Reprinted from Genovese and Rao (2003a), with permission from AACC International.

Unfortunately, the reasons/mechanisms of that yielding behavior were not clear, and no theoretical models were proposed in those works.

Colloidal dispersions. Volume fraction (ϕ) and particle size (d) affect the density of the interparticle links and the microstructure, which in turn govern the yield stress behavior of concentrated colloidal dispersions (Zhou and others 2001). Consequently, most theoretical yield stress models are mainly functions of ϕ, d, and particle–particle interactions. A representative selection of the many models found in the literature is presented next.

Michaels and Bolger (1962) derived the following expression for suspensions of aggregated flocs, where the aggregates form tenuous networks

$$\sigma_0 = F\frac{H}{d^2}\left(\phi - \phi_f\right)^3 \tag{19}$$

where σ_0 is the apparent yield stress, F is a dimensionless orientation function, H is the interfloc adhesive force, d is the diameter of the individual flocs, and ϕ_f is the minimum floc concentration required to form a continuous aggregate network.

By considering the colloidal interparticle forces, Poslinski and others (1988) derived an expression for the yield stress of solid spheres dispersed in a polymeric matrix

$$\sigma_0 = \frac{ZA}{8\pi d^3}\left[1 - \frac{\phi}{\phi_m}\right]^{-4} + \frac{3Z\varepsilon\varepsilon_0\kappa\psi_0^2}{4\pi d} \tag{20}$$

where Z is the total number of nearest neighbors of each sphere in a particular packing configuration, A is the Hamaker constant (a measure of the van der Waals attractive forces), ε is the dielectric constant of the continuous medium, ε_0 the permittivity of vacuum, and ψ_0 is the surface potential of the spheres. The 2nd term in Eq. 20 accounts for the electrostatic repulsive forces.

Scales and others (1998) proposed a general interactive model for the shear yield stress of flocculated suspensions. For monodisperse spherical particles, the model reduces to an expression similar to Eq. 20:

$$\sigma_0 = \frac{\phi \cdot M(\phi)}{24\pi d}\left[\frac{A}{r^2} - \frac{24\pi\varepsilon\varepsilon_0\kappa\zeta^2}{1+\exp(\kappa r)}\right] \tag{21}$$

where $M(\phi)$ is the mean coordination number. The terms in the bracket account for the van der Waals and EDL forces acting between pairs of particles, or the strength of 1 particle bond.

For polydisperse spheres, the previous model is quite complex and may be consulted in the work of Scales and others (1998). A simpler model has been suggested for calculation of the yield stress of a mixture suspension (Zhou and others 2001):

$$\sigma_0 = \left(\sum \frac{\phi_i}{\phi}\sqrt{\sigma_{0_i}}\right)^2 \tag{22}$$

where ϕ_i and σ_{0i} are the volume fraction and yield stress of the ith component of the suspension, respectively. Unlike hard-sphere dispersions in which polydispersity reduces the viscosity (Eq. 5), a suspension with a broad particle size distribution exhibits higher yield stress than a narrow size distributed suspension (Zhou and others 2001).

From Eq. 12, Buscall (1991, 1994) derived Eq. 23, in which the yield stress arises when the effective particle radius is high enough to produce a dense packing of particles, thus

$$\sigma_0 \approx \frac{K(\phi_{eff})}{a_m^3}\left[U\left(2a_m\right) - k_B T\right] \tag{23}$$

where a_m is the maximum radius that the particle can take because of the spatial constraints of the other particles, and the other terms are the same as in Eq. 12.

Based on Eq. 9, Ogawa and others (1997) proposed a simpler model, indicating that when the effect of repulsive interaction is strong, there is an apparent yield stress given by

$$\sigma_0 = \frac{\phi \cdot U(r)}{c_1 d^3} \tag{24}$$

It should be noted that Eq. 20 and 21 only consider DLVO (van der Waals and repulsive electrostatic) interparticle forces, while Eq. 23 and 24 are functions of the total interaction potential, U, which may include also non-DLVO (steric, hydration, depletion, and so on) interactions.

From analyses of experimental data and theoretical analysis from several works, Zhou and others (2001) suggested the following general expression:

$$\sigma_0 = B\frac{\phi^v}{d^2} \tag{25}$$

where constant B is related with bond strength depending on material properties and system surface chemistry condition.

The power-law exponent in Eq. 25, v, has been correlated with the fractal dimension, which is believed to be associated with the interconnection and space-filling ability of the network microstructure. To describe this behavior, de Rooij and others (1994) developed a microrheological model in terms of fractal microstructures (Eq. 26):

$$\sigma_0 \propto \phi^{3/(3-D_f)} \tag{26}$$

This model describes the suspension in terms of particle chains where interparticle bonds can be soft or rigid, similar to the study of Shih and others (1990) (Eq. 18).

Finally, it is worth mentioning the model of Berli and Quemada (2000) for microgel suspensions (Eq. 15 to 17), where the yield stress is simply given by

$$\sigma_0 = \chi\sigma_c \tag{27}$$

which is only valid if $\phi > \phi_0$ approximately ϕ_{m}, that is, when particles are densely packed.

The differences among Eq. 19 to 27 suggest that there is not a unique or general theoretical model to describe the yield stress

Table 2—Fractal dimension of structural elements in a few foods based on rheological data (Rao 2006)

Network of particles	Fractal dimension, D_f	Reference
Palm oil or lard fat	2.82–2.88	Marangoni and Rousseau (1998)
Cocoa butter	2.37	Narine and Marangoni (1999)
Salatrim®	2.90	Narine and Marangoni (1999)
Milk fat and / canola oil blends	1.97–1.99	Marangoni and Hartel (1998)
Whey protein isolate + $CaCl_2$ gels	2.3–2.6	Hongsprabhas and others (1999)
Soy protein isolate gels, pH 3.8 and 0.2M NaCl	2.3.	Renkema and van Vliet (2004)
Starch gels	2.79–2.81	Genovese and Rao (2003a)
Egg white protein gel, pH 3.7	1.9–2.1	Ould-Eleya and others 2004

of concentrated colloidal dispersions, but instead the appropriate model should be chosen/derived for each particular system.

Foams. Foams behave as elastic solids under small deformations, and flow like viscous liquids above a certain yield stress (Pernell and others 2000; Kampf and others 2003). Based on Eq. 25 and other models for foams (Höhler and others 1999; Princen and Kiss 1989; Davis and others 2004), Raharitsifa and others (2006) proposed a generalized expression for the yield stress of foams as a function of their structural properties:

$$\sigma_0 = B' \frac{\phi^v}{D_{32}^b} \tag{28}$$

where ϕ is the air volume fraction, parameter B' is expected to include the effect of interfacial tension, b is a fitting parameter, and D_{32} is the Sauter mean bubble diameter or surface average diameter. For spherical bubbles

$$D_{32} = \sum d_i^3 \Big/ \sum d_i^2 \tag{29}$$

where d_i is the diameter of each bubble, and i varies from 1 to the number of bubbles observed. Raharitsifa and others (2006) applied Eq. (28) to experimental data (Figure 5) on apple juice foams prepared with different concentrations of 2 different foaming agents (methylcellulose and egg white), resulting in B' =18.9, v =10.9, and b =1.37 (R^2 =0.975).

Structural Models and Analyses

Structural models

These models are derived from consideration of the structure and often kinetics of changes in it. They are used, together with experimental data, to estimate values of parameters that help characterize the rheological behavior of a food sample. One such model is that of Cross (1965) (Eq. 30) that has been used extensively to characterize the flow behavior of polymer dispersions and other shear-thinning fluids.

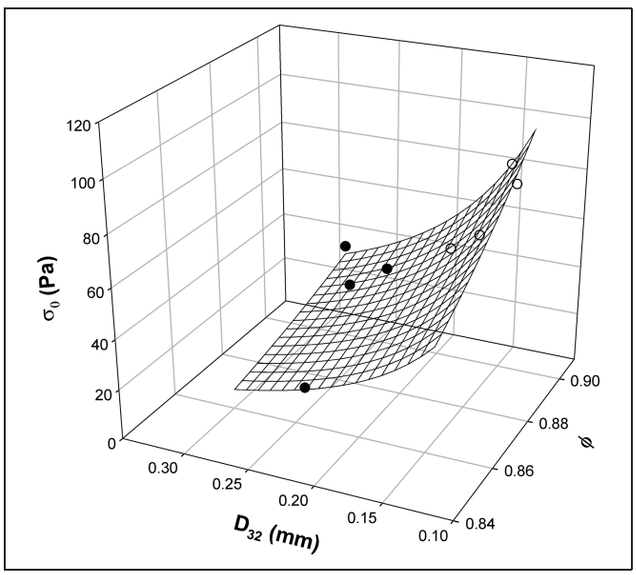

Figure 5—Yield stress of apple juice foams as function of air volume fraction and bubble mean diameter for different foaming agents: (•) methylcellulose, and (○) egg white. Experimental data (symbols) fitted with Eq. 28 (mesh). From Raharitsifa and others (2006).

$$\eta_a = \eta_\infty + \frac{\eta_0 - \eta_\infty}{1 + (\alpha_c \dot{\gamma})^m} \tag{30}$$

For the shear rate, $\dot{\gamma}_c$, where $\eta_a = (\eta_0 + \eta_\infty)/2$, the Cross time constant $\alpha_c = 1/\dot{\gamma}_c$. Generally, $\dot{\gamma}_c$ gives an order of magnitude of the critical shear rate marking the end of the zero shear rate Newtonian plateau or the onset of the shear-thinning region (Rao 1999).

The Casson model (Eq. 31) is another structure-based model (Casson 1959) that, although developed for characterizing printing inks originally, has been used to characterize chocolate and other food dispersions that exhibit yield stress.

$$\sigma^{0.5} = K_{0c} + \mathrm{K}_c\,(\dot{\gamma})^{0.5} \tag{31}$$

From a $\sigma^{0.5}$ compared with $\dot{\gamma}^{0.5}$ plot, the Casson yield stress is calculated as the square of the intercept, $\sigma_{0c} = (K_{0c})^2$ and the Casson plastic viscosity as the square of the slope, $\eta_{Ca} = (K_c)^2$.

Structural analyses

While application of structure-based models to rheological data does provide useful information, structure-based analysis can provide valuable insight into the role of the structure of a dispersed system. Bodenstab and others (2003) estimated the contributions to flow shear stress of soy milk by suspended particles and the suspending fluid.

$$\sigma = \sigma_s + \sigma_p \tag{32}$$

where σ_s is the shear stress caused by the viscous forces generated by the suspending fluid (continuous phase), and σ_p is the shear stress caused by interaction between suspended particles. The former is temperature dependent and in the latter the temperature dependency can be neglected. In the direct interparticle interactions, Coulomb's mechanical friction forces, hydrogen bonds, electrostatic attraction, and hydrophobic attraction may be important. The viscous contribution was estimated from the expression

$$\sigma_s = \eta_s \frac{\sigma_1 - \sigma_2}{\eta_1 - \eta_2} \tag{33}$$

where the subscripts 1 and 2 refer to the values of stress and viscosity of the dispersion at temperatures 1 and 2, respectively. Typical values of temperature that were used were 10 °C and 25 °C, and 20 °C and 40 °C (Bodenstab and others 2003). Considerable care had to be used to obtain reliable samples of the continuous phase of the soy milk without solid residues, a concern with many other food dispersions such as fruit and vegetable products (Rao 1987). Another concern is that significant differences in structure of the sample may exist at the 2 different temperatures used. Nevertheless, for the soy milks, interparticle interactions were found to be significant at particle concentrations above about 20 g/100 g.

In the kinetic or structural approach to rheology of dispersions (Michaels and Bolger 1962), the basic flow units are assumed to be small clusters or flocs that at low shear rates give the dispersion a finite yield stress. The clusters associate randomly to form weakly bonded aggregates and tenuous networks, giving rise to plastic and structural properties. Based on the work of Michaels and Bolger (1962), from an energy balance at the point of maximum deformation (yield point) in the vane test, the contributions of different structural components to the total yield stress, σ_{0s}, may be estimated (Genovese and Rao 2003b)

$$\sigma_{0s} = \sigma_b + \sigma_v + \sigma_n \quad (34)$$

The stress to break the bonds between the flocs may be calculated as the difference between the static, σ_{0s}, and the dynamic, σ_{0d}, yield stresses of the samples with undisrupted and disrupted structure, respectively.

$$\sigma_b = \sigma_{0s} - \sigma_{0d} \quad (35)$$

where σ_b is the stress required to break the bonds between the flocs, σ_v is the stress dissipated due to purely viscous drag, and σ_n is the stress required to break the aggregate network. Given that $\sigma_v = \eta_\infty \dot{\gamma}$ is very small in most dispersions, one can estimate the 2 contributions σ_b and σ_n. As 1 example of structural analysis of processed foods, the contribution of bonding to the static yield stress of products that were homogenized, such as mayonnaise, ranged between 53% and 65%, while that of finished, nonhomogenized products such as apple sauce was about 20% (Genovese and Rao 2005). In another study (Tárrega and others 2006), the influence of starch concentration and λ-carrageenan on the contribution of bonding in skim milk-based dispersions was examined.

A texture map can be created by plotting yield stress values against the corresponding values of the deformation. The texture map of 3 heated starch dispersions based on static and dynamic yield stresses compared with deformation is shown in Figure 6 (Genovese and Rao 2003b). Unlike a traditional texture map, a map based on static and dynamic yield stresses indicates the behavior of a food with both undisrupted and disrupted structure, and should be valuable in evaluation of product quality.

Conclusions

Some food dispersions (for example, cloudy apple juice) contain colloidal particles with dimensions $< 10\ \mu$m, and others (for example, tomato concentrates, orange juice) contain larger, noncolloidal particles with dimensions $> 10\ \mu$m. Theoretical models have been derived assuming that the particles are rigid to predict viscosity, yield stress, and modulus of both types of dispersions.

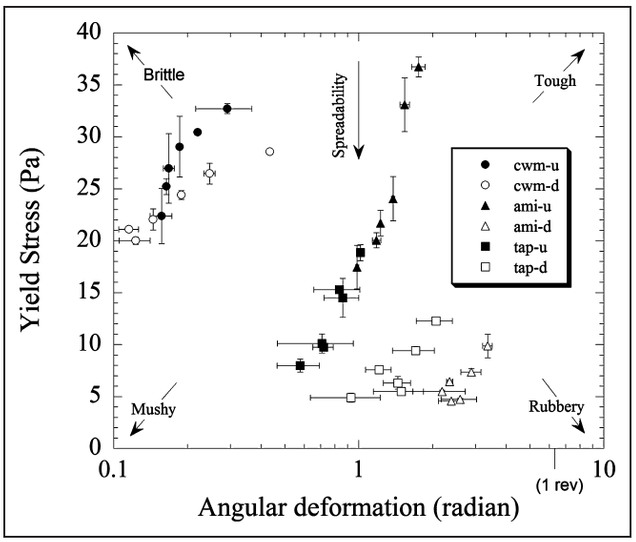

Figure 6 — Texture map of cross-linked waxy maize (cwm), amioca (ami), and tapioca (tap) starch dispersions with undisrupted (u) and disrupted (d) structures. From Genovese and Rao (2003b).

These models provide valuable guidelines with respect to the role of key rheological parameters such as volume fraction, size, and fractal dimension of the particles, as well as interparticle forces. However, due to the complex, including nonrigid, nature of particles in most food dispersions, those models have been modified to describe viscosity data. Also due to the complex structure of foods, structural analyses have been developed that are based on experimental rheological data on dispersions and they provide insight into the nature of food microstructure.

Finally, it is worth to mention that foods are subjected to extensional shear in the mouth and in some unit operations (such as fiber spinning and dough mixing). Therefore, extensional viscosity and its measurement are also of interest. Briefly, for low-viscosity fluids, techniques based on creating a stagnation point such as flow between opposing jets and filament stretching have been developed. For high-viscosity and semisolid foods, biaxial (compression-extension) deformation technique has been used (Rao 1999). Further, to better understand how food structure deforms under elongational flow at the microscale, equipment was developed to visualize food structure behavior under compression–extension deformation by combining confocal microscopy and compression apparatus (Nicolas and Paques 2003). One can anticipate that more rheo-optical studies will be conducted, which should provide both visual and rheological data on foods at the microscale.

Acknowledgments

Authors Genovese and Lozano are grateful for financial support from CONICET. Author Rao acknowledges support from USDA-NRI competitive grants.

Nomenclature

a = particle radius, m
a_m = maximum particle radius, m
A = Hamaker constant, J
b = constant in Eq. 28, dimensionless
B, B' = constants in Eq. 25 and 28, N and N.m^{b-2}, respectively
c = dry starch concentration, dimensionless
c_1, c_2 = constants in Eq. 9, dimensionless
d = particle diameter, m
D = Euclidean dimension, dimensionless
D_f = fractal dimension, dimensionless
D_{32} = Sauter mean diameter of bubbles, m
F = orientation function, dimensionless
G' = elastic modulus, Pa
G'_0 = plateau modulus, Pa
H = interfloc adhesive force, N
k = phenomenological factor in Eq. 12, dimensionless
$\bar{k}_a$ = aggregation rate constant, s^{-1}
k_B = Boltzmann constant, J/°K
K = phenomenological factor in Eq. 12, dimensionless
K_C = square root of Casson plastic viscosity, (Pa.s)$^{1/2}$
K_{0c} = square root of Casson yield stress, Pa$^{1/2}$
m = Cross exponent, dimensionless
M = mean coordination number, dimensionless
N = averaged number of particles in a cluster, dimensionless
p = primary electroviscous effect coefficient, dimensionless
q = axial ratio, dimensionless
Q = swelling factor, dimensionless
r = distance between pairs of particles, m
t, t_0 = time, initial time, s
T = absolute temperature, °K
U = total interaction potential between pairs of particles, J
U_{Max} = energy barrier between pairs of particles, J

v = constant in Eq. 25 and 28, dimensionless
Z = total number of nearest neighbors of each sphere, dimensionless

Greek Letters

α = constant in Eq. 8, dimensionless
α_C = Cross time constant, s
β = constant in Eq. 4, dimensionless
$\dot{\gamma}$ = shear rate, s^{-1}
$\dot{\gamma}_c$ = critical shear rate, s^{-1}
ε = dielectric constant of the continuous medium, dimensionless
ε_0 = permittivity of vacuum, F/m
ζ = zeta potential, V
η = dispersion viscosity, Pa.s
η_a = apparent viscosity, Pa.s
η_m = filling medium viscosity, Pa.s
η_r = relative viscosity, dimensionless
η_s = solvent viscosity, Pa.s
η_0 = zero-shear viscosity (apparent viscosity as $\dot{\gamma} \to 0$), Pa.s
η_∞ = infinite-shear viscosity (apparent viscosity as $\dot{\gamma} \to \infty$), Pa.s
$[\eta]$ = intrinsic viscosity, dimensionless
κ = reciprocal Debye length, m^{-1}
σ = shear stress, Pa
σ_b = shear stress required to break the bonds between flocs, Pa
σ_c = critical shear stress, Pa
σ_n = stress required to break the aggregate network, Pa
σ_p = shear stress caused by particle interaction, Pa
σ_s = shear stress caused by flow of the suspending fluid, Pa
σ_v = shear stress dissipated due to purely viscous drag, Pa
σ_0 = yield stress, Pa
σ_{0d} = dynamic yield stress, Pa
σ_{0s} = static yield stress, Pa
ϕ = volume fraction of the dispersed phase, dimensionless
ϕ_f = minimum floc volume fraction, dimensionless
ϕ_m = maximum packing fraction, dimensionless
ϕ_0, $\phi_\infty = \phi_m$ for $\sigma \to 0$ and $\sigma \to \infty$,
χ = rheological index, dimensionless
ψ_0 = surface potential, V

Subscripts

cf = colloidal forces
eff = effective
hs = hard-sphere

References

Barnes HA. 2000. A handbook of elementary rheology. 1st ed. Wales: Cambrian Printers. 200 p.
Benítez E, Genovese DB, Lozano JE. 2007. Effect of pH and ionic strength on apple juice turbidity: application of the extended DLVO theory. Food Hydrocoll 21(1):100–9.
Berli CLA, Quemada D. 2000. Prediction of the interaction potential of microgel particles from rheometric data. Comparison with different models. Langmuir 16:10509–14.
Berli CLA, Deiber JA, Añón MC. 1999a. Connection between rheological parameters and colloidal interactions of a soy protein suspension. Food Hydrocoll 13:507–15.
Berli CLA, Deiber JA, Añón MC. 1999b. Heat-induced phenomena in soy protein suspensions. Rheometric data and theoretical interpretation. J Agric Food Chem 47:893–900.
Bodenstab S, Juillerat M, Bauer W, Sommer K. 2003. Separating the role of particles and the suspending fluid for the flow of soy milks. J Food Sci 68(5):1722–30.
Buscall R. 1991. Effect of long-range repulsive forces on the viscosity of concentrated lattices: comparison of experimental data with an effective hard-sphere model. J Chem Soc Faraday Trans 87:1365–70.
Buscall R. 1994. An effective hard-sphere model of the non-Newtonian viscosity of stable colloidal dispersions: comparison with further data for sterically stabilized lattices and with data for microgel particles. Coll Surf A 83:33–42.
Casson N. 1959. A flow equation for pigment-oil suspensions of the printing ink type. In: Mill CC, editor. Rheology of disperse systems. New York: Pergamon Press. p 82–104.
Cross MM. 1965. Rheology of non-Newtonian fluids: a new flow equation for pseudoplastic systems. J Colloid Sci 20:417–37.
Davis JP, Foegeding EA, Hansen FK. 2004. Electrostatic effects on the yield stress of whey protein isolate foams. Coll Surf B: Biointerf 34:13–23.
De Rooij R, Potanin A, van den Ende D, Mellema J. 1994. Elasticity of weakly aggregating polystyrene latex dispersions. Phys Rev E 49(4):3038–49.
Farris RJ. 1968. Prediction of the viscosity of multimodal suspensions from unimodal viscosity data. Trans Soc Rheol 12(2):281–301.
Genovese DB, Lozano JE. 2006. Contribution of colloidal forces to the viscosity and stability of cloudy apple juice. Food Hydrocoll 20:767–73.
Genovese DB, Rao MA. 2003a. Role of starch granule characteristics (volume fraction, rigidity and fractal dimension) on the rheology of starch dispersions with and without amylose. Cereal Chem 80:350–5.
Genovese DB, Rao MA. 2003b. Vane yield stress of starch dispersions. J Food Sci 68(7):2295–301.
Genovese DB, Rao MA. 2005. Components of vane yield stress of structured food dispersions. J Food Sci 70(8):E498–504.
Gondret P, Petit L. 1997. Dynamic viscosity of macroscopic suspensions of bimodal sized solid spheres. J Rheol 41:1261–74.
Herzhaft B. 1999. Rheology of aqueous foams: a literature review of some experimental works. Oil Gas Sci Technol 54(5):587–96.
Hidalgo-Álvarez R, Martín A, Fernández A, Bastos D, Martínez F, de las Nieves FJ. 1996. Electrokinetic properties, colloidal stability and aggregation kinetics of polymer colloids. Adv Coll Interf Sci 67:1–118.
Höhler R, Cohen-Addad S, Asnacios A. 1999. Rheological memory effect in aqueous foams. Europhys Lett 48(1):93–8.
Hongsprabhas P, Barbut S, Marangoni AG. 1999. The structure of cold-set whey protein isolate gels prepared with Ca^{++}. Lebensm Wiss U Technol 32(4):196–202.
Husband DM, Aksel N, Gleissle W. 1993. The existence of static yield stresses in suspensions containing noncolloidal particles. J Rheol 37(2):215–35.
Kampf N, Gonzalez MC, Corradini MG, Peleg M. 2003. Effect of two gums on the development, rheological properties and stability of egg albumen foams. Rheol Acta 42:259–68.
Kitano T, Kataoka T, Shirota T. 1981. An empirical equation of the relative viscosity of polymer melts filled with various inorganic fillers. Rheol Acta 20:207–9.
Krieger IM, Dougherty TJ. 1959. A mechanism for non-Newtonian flow in suspensions of rigid spheres. Trans Soc Rheol 3:137–52.
Liao H-J, Tattiyakul J, Rao MA. 1999. Superposition of complex viscosity curves during gelatinization of starch dispersion and dough. J Food Process Eng 22:215–34.
Mandelbrot BB. 1982. The fractal geometry of nature. New York: WH Freeman.
Marangoni AG, Hartel RW. 1998. Visualization and structural analysis of fat crystal networks. Food Technol 52(9):46–51.
Marangoni AG, Rousseau D. 1998. The influence of chemical interesterification on the physicochemical properties of complex fat systems. III. Rheology and fractality of the crystal network. J Am Oil Chemists Soc 75(11):1633–6.
Marquez M, Robben A, Grady BP, Robb I. 2006. Viscosity and yield stress reduction in noncolloidal concentrated suspensions by surface modification with polymers and surfactants and/or nanoparticle addition. J Coll Interf Sci 295: 374–87.
Martínez-Padilla LP. 2005. Food suspensions. In Barbosa-Cánovas GV, editor. Food engineering. France: EOLSS Publishers, UNESCO. p 323–38
McClements DJ. 1999. Food emulsions: principles, practice, and techniques. Boca Raton, Fla.: CRC Press.
Metzner AB. 1985. Rheology of suspensions in polymeric liquids. J Rheol 29(6):739–75.
Michaels AS, Bolger JC. 1962. The plastic flow behavior of flocculated kaolin suspensions. I&EC Fund 1:153–62.
Narine SS, Marangoni A. 1999. The difference between cocoa butter and salatrim lies in the microstructure of the fat crystal network. J Am Oil Chemists Soc 76(1): 7–13.
Nicolas Y, Paques M. 2003. Microrheology: an experimental technique to visualize food structure behavior under compression-extension deformation conditions. J Food Sci 68(6):1990–4.
Ogawa A, Yamada H, Matsuda S, Okajima K. 1997. Viscosity equation for concentrated suspensions of charged colloidal particles. J Rheol 41(3):769–85.
Ould-Eleya MM, Ko S, Gunasekaran S. 2004. Scaling and fractal analysis of viscoelastic properties of heat-induced protein gels. Food Hydrocoll 18(2):315–23.
Pernell CW, Foegeding EA, Daubert CR. 2000. Measurement of the yield stress of protein foams by vane rheometry. J Food Sci 65(1):110–4.
Pernell CW, Foegeding EA, Luck PJ, Davis JP. 2002. Properties of whey and egg white protein foams. Coll Surf A 204:9–21.
Poslinski AJ, Ryan ME, Gupta RK, Seshadri SG, Frechette FJ. 1988. Rheological behavior of filled polymeric systems I. Yield stress and shear-thinning effects. J Rheol 32(7):703–35.
Princen HM, Kiss AD. 1989. Rheology of foams and highly concentrated emulsions. J Coll Interf Sci 128(1):176–87.
Quemada D, Berli C. 2002. Energy of interaction in colloids and its implications in rheological modeling. Adv Coll Interf Sci 98: 51–85.
Qin K, Zaman AA. 2003. Viscosity of concentrated colloidal suspensions: comparison of bidisperse models. J Coll Interf Sci 266:461–7.
Raharitsifa N, Genovese DB, Ratti C. 2006. Characterization of apple juice foams for foam-mat drying prepared with egg white protein and methylcellulose. J Food Sci 71(3):E142–51.
Rao MA. 1987. Predicting the flow properties of food suspensions of plant origin: Mathematical models help clarify the relationship between composition and rheological behavior. Food Technol 41(3):85–8.
Rao MA. 1999. Rheology of fluid and semisolid foods: principles and applications. Gaithersburg, Md: Aspen Publishers. p 433.
Rao MA. 2006. Influence of food microstructure on food rheology. In: McClements DJ, editor. Understanding and controlling the microstructure of complex foods. Cambridge, U.K.: Woodhead Publishing Ltd..
Renkema JMS, van Vliet T. 2004. Concentration dependence of dynamic moduli of heat-induced soy protein gels. Food Hydrocoll 18(3):483–7.
Rubio-Hernández FJ, Carrique F, Ruiz-Reina E. 2004. The primary electroviscous effect in colloidal suspensions. Adv Coll Interf Sci 107:51–60.
Russel WB. 1980. Review of the role of colloidal forces in the rheology of suspensions. J Rheol 24(3):287–317.

Russel WB, Saville DA, Schowalter WR. 1989. Colloidal dispersions. Ed. G.K. Batchelor. Cambridge, U.K.: Cambridge Univ. Press. p.525.
Scales PJ, Kapur PC, Johnson SB, Healy TW. 1998. Shear yield stress of partially flocculated colloidal suspensions. AIChE J 44(3):538–44.
Sennet P, Olivier JP. 1965. Colloidal dispersions, electrokinetic effects, and the concept of zeta potential. In Gushee DE editor. Chemistry and physics of interfaces. Washington D.C.: American Society Publications. p 73–92.
Servais C, Jones R, Roberts I. 2002. The influence of particle size distribution on the processing of food. J Food Eng 51:201–8.
Shih W-H, Shih WY, Kim S-I, Liu J, Aksay IA. 1990. Scaling behavior of the elastic properties of colloidal gels. Phys Rev A 42(8):4772–9.
Steffe JF. 1996. Rheological methods in food process engineering. 2nd ed. East Lansing, Mich.: Freeman Press. p 418.
Tanglertpaibul T, Rao MA. 1987. Rheological properties of tomato concentrates as affected by particle size and methods of concentration. J Food Sci 52:141–5.
Tárrega A, Costell E, Rao MA. 2006. Vane yield stress of native and cross-linked starch dispersions in skim milk: effect of starch concentration and λ-carrageenan addition. Food Sci Tech Int 12(3):253–60.
Tattiyakul J, Rao MA. 2000. Rheological behavior of cross-linked waxy maize starch dispersions during and after heating. Carbohydr Polym 43:215–22.
Thakur RK, Vial C, Djelveh G. 2003. Influence of operating conditions and impeller design on the continuous manufacturing of food foams. J Food Proc Eng 60:9–20.
Tsai SC, Zammouri K. 1988. Role of interparticular van der Waals force in rheology of concentrated suspensions. J Rheol 32(7):737–50.
Vernon-Carter EJ, Espinosa-Paredes G, Beristain CI, Romero-Tehuitzil H. 2001. Effect of foaming agents on the stability, rheological properties, drying kinetics and flavour retention of tamarind foam-mats. Food Res Int 34:587–98.
Vitali AA, Rao MA. 1984. Flow properties of low-pulp concentrated orange juice: serum viscosity and effect of pulp content. J Food Sci 49(3):876–81.
Yang WH, Rao MA. 1998. Complex viscosity-temperature master curve of cornstarch dispersion during gelatinization. J Food Proc Eng 21:191–207.
Yoo B, Rao MA 1996. Creep and dynamic rheological behavior of tomato concentrates: effect of concentration and finisher screen size. J Texture Stud 27:451–9.
Zhou Z, Scales PJ, Boger DV. 2001. Chemical and physical control of the rheology of concentrated metal oxide suspensions. Chem Eng Sci 56:2901–20.